Sixth International Symposium on Turbulence and Shear Flow Phenomena
Seoul, Korea, 22-24 June 2009

DIRECT NUMERICAL SIMULATION OF THE COMPRESSIBLE KELVIN-HELMHOLTZ INSTABILITY WITH A LOW-DISSIPATION SHARP-INTERFACE METHOD

X. Y. Hu and N. A. Adams
Lehrstuhl für Aerodynamik, Technische Universität München
85748 Garching, Germany
Xiangyu.Hu@aer.mw.tum.de

Q. Wang
Chinese Academy of Aerospace Aerodynamics
100074 Beijing, China

ABSTRACT

In this paper, a sharp-interface method combined with a low-dissipation weighted essential non-oscillatory (WENO) scheme is introduced to simulate the compressible Kelvin-Helmholtz instability. As the material interface is described as a contact discontinuity, this method resolves the exact tangential velocity discontinuity. By normalizing the original smoothness indicators with that of the optimal stencil, a modified WENO method with low dissipation is developed. While still keeping good shock-capturing properties, the modified method decreases the over damping in moderate flow field considerably, and is able to achieve comparable accuracy as that of hybrid methods. Different from previous simulations with single fluid or miscible interface methods, which suppress the high-wave-number modes by initially prescribed finite-width shear layer or fast numerical dissipation, this method allows the development of high-wave-number perturbation. However, the simulations still suggest that the high-wave-number perturbation shown different behavior from previous simulations and linear theory on idea KH instability but resemble those on shear layer with finite thickness.

INTRODUCTION

The Kelvin-Helmholtz (KH) instability caused by tangential velocity discontinuity is a fundamental problem, and has been a subject of study for many years. The KH instability plays important roles in the evolution of mixing layer and the transition to turbulence. The idea KH instability evolves from tangential velocity discontinuity, and is independent of fluid viscosity and may also involve with material interface and fluid compressibility. Since the analytical analysis usually can only study the very early linear and weak non-linear stage, numerical simulation is essential for understanding the strong non-linear behavior in the later stage.

When the considered flows are compressible, while some closely related phenomena, such as high-speed shear or mixing layers, have been numerically studied extensively, there are still several challenges for the direct numerical simulation of the KH instability. One difficulty is the numerical representation of the tangential velocity discontinuity and the treatment of the material interface. Another difficulty is that, in order to handle shock waves developed in the instabilities, shock-capturing schemes, like the weighted essential non-oscillatory (WENO) scheme, are need to be used. However, it is well known that these scheme are much more dissipative than the center-difference type schemes, like compact scheme, which are not numerically stable near the shock waves. For example, the adaption mechanism of WENO scheme is overly sensitive to moderate flow field which do not require shock-capturing. The reason is that the effective interpolation modulated by the weights reaches that of the optimal stencil very slowly, which leads to over-dissipation in the regions without strong-shock but large density variation and shear rate.

In a recent study we have developed a level-set conservative sharp-interface method for compressible flows, which is capable of calculating the complex evolution of the material interface stably and accurately (Hu et al 2006). This method has been successfully used for the direct numerical simulation of the Richtmyer-Meshkov instability (Hu et al. 2007). In this paper, this method is combined with a low-dissipation WENO scheme to simulate the KH instability. As the material interface is described as a contact discontinuity, the presented method resolves the exact tangential velocity discontinuity (equivalent to a zero-thickness vortex sheet). This method allows the development of high-wave-number perturbation, and is different from previous simulations with single fluid or miscible interface methods, in which the high-wave-number modes are suppressed by initially prescribed finite-width shear layer or fast numerical dissipation.

SHARP-INTERFACE METHOD

Assuming the fluid is inviscid and compressible the governing equation of the flow can be written as a system of conservation laws

$$\frac{\partial \mathbf{U}}{\partial t} + \nabla \cdot \mathbf{F} = 0 \quad \text{on } \Omega, \tag{1}$$

where $\mathbf{U}$ is the density of the conserved quantities of mass, momentum and total energy, and $\mathbf{F}$ represents the corresponding flux functions. When an interface $\Gamma(t)$ separates the domain Ω into two sub-domains $\Omega^1(t)$ and $\Omega^2(t)$, as for a multi-fluid problem, the evolution of the interface is determined by the interface condition defined by a two-material Riemann problem

$$\mathcal{R}(\mathbf{U}_{fluid1}, \mathbf{U}_{fluid2}) = 0 \quad \text{on } \Gamma(t). \tag{2}$$

Following Miller and Colella (2002), we consider Eq. (1) for the fluid occupying the sub-domain Ω^1 on a two-dimensional Cartesian grid with grid spacings Δx and Δy. A finite volume discretization can be obtained from integrating Eq. (1) over the space-time volume $\Delta_{ij} \bigcap \Omega^1(t)$ of a computational cell (i,j) occupied by the fluid

$$\int_n^{n+1} dt \int_{\Delta_{ij} \bigcap \Omega^1(t)} dxdy \left(\frac{\partial \mathbf{U}}{\partial t} + \nabla \cdot \mathbf{F} \right) = 0 \quad (3)$$

where $\Delta_{ij} = \Delta x \Delta y$ is the cell volume. $\Delta_{ij} \bigcap \Omega^1(t)$ can be represented by $\alpha_{i,j}(t)\Delta x \Delta y$ where $\alpha_{i,j}(t)$ is the time dependent volume fraction of the considered fluid and satisfying $1 \geq \alpha \geq 0$. By an application of Gauss's theorem, one obtains

$$\int_n^{n+1} dt \int_{\Delta_{ij} \bigcap \Omega^1(t)} dxdy \frac{\partial \mathbf{U}}{\partial t} + \int_n^{n+1} dt \int_{\partial \Delta_{ij} \bigcap \Gamma(t)} dxdy \mathbf{F} \cdot \mathbf{n} = 0 \quad (4)$$

where $\partial \Delta_{ij}$ are the four cell faces intersecting orthogonally with the grid at four locations $(x_i + \Delta x/2, y_j)$, $(x_i, y_j + \Delta y/2)$, $(x_i - \Delta x/2, y_j)$ and $(x_i, y_j - \Delta y/2)$. Denoting the

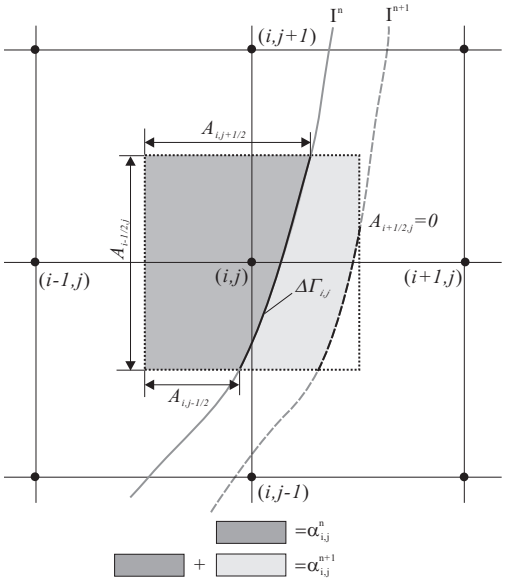

Figure 1: Schematic of conservative discretization for a cut cell.

interface location as $\Gamma(t)$, as shown in Fig. 1, $\partial \Delta_{ij} \bigcap \Gamma(t)$ can be represented by two parts: one is the combination of the four segments of the cell faces being cut by the interface, which can be written in the form of $A_{i+1/2,j}(t)\Delta y$, $A_{i,j+1/2}(t)\Delta x$, $A_{i-1/2,j}(t)\Delta y$ and $A_{i,j-1/2}(t)\Delta x$ where $1 \geq A \geq 0$ is the aperture; the other one is the segment of the interface $\Delta\Gamma_{i,j}(t)$ inside of the cell (i,j). Hence, Eq. (4) can be rewritten as

$$\begin{aligned} &\left(\alpha_{i,j}^{n+1}\mathbf{U}_{i,j}^{n+1} - \alpha_{i,j}^{n}\mathbf{U}_{i,j}^{n}\right)\Delta t = \\ &\int_n^{n+1} dt \frac{1}{\Delta x}\left[A_{i+1/2,j}(t)\hat{\mathbf{F}}_{i+1/2,j} - A_{i-1/2,j}(t)\hat{\mathbf{F}}_{i-1/2,j}\right] \\ +\ &\int_n^{n+1} dt \frac{1}{\Delta y}\left[A_{i,j+1/2}(t)\hat{\mathbf{F}}_{i,j+1/2} - A_{i,j-1/2}(t)\hat{\mathbf{F}}_{i,j-1/2}\right] \\ +\ &\int_n^{n+1} dt \frac{1}{\Delta x \Delta y}\hat{\mathbf{X}}\left[\Gamma_{i,j}(t)\right] \end{aligned} \quad (5)$$

where $\alpha_{i,j}(t)\mathbf{U}_{i,j}$ and $\mathbf{U}_{i,j}$ are the conservative quantities in the cut cell and the cell-averaged density of conservative quantities of the considered fluid, respectively. $\hat{\mathbf{F}}$ is the average cell-face flux and $\hat{\mathbf{X}}\left[\Gamma_{i,j}(t)\right]$ is the average momentum and energy exchange across the interface segment determined by the interface interaction of Eq. (2). With explicit first-order forward time difference, the above equation can be approximated as

$$\begin{aligned} \alpha_{i,j}^{n+1}\mathbf{U}_{i,j}^{n+1} &= \alpha_{i,j}^{n}\mathbf{U}_{i,j}^{n} \frac{\Delta t}{\Delta x \Delta y} + \hat{\mathbf{X}}(\Delta\Gamma_{i,j}) \\ +\ &\frac{\Delta t}{\Delta x}\left[A_{i-1/2,j}\hat{\mathbf{F}}_{i-1/2,j} - A_{i+1/2,j}\hat{\mathbf{F}}_{i+1/2,j}\right] \\ +\ &\frac{\Delta t}{\Delta y}\left[A_{i,j-1/2}\hat{\mathbf{F}}_{i,j-1/2} - A_{i,j+1/2}\hat{\mathbf{F}}_{i,j+1/2}\right] \end{aligned} \quad (6)$$

where Δt is the time step size. Note that all the terms on the right-hand-side are evaluated at time step n. Also note that a Runge-Kutta scheme can be employed for higher order time integration while maintaining discrete conservation since every Runge-Kutta sub-step can be formulated as Eq. (6).

Interface description

We associate the computational domain Ω with a signed distance function $\phi(x,y,t)$, that is $\nabla|\phi| = 1$, called the level set function (Osher and Sethain 1988). Knowing ϕ we may locate the interface by finding the zero level set of ϕ. That is $\Gamma(t) = \{x, y : \phi(x,y,t) = 0\}$ which divides the entire domain into two sub-domains, each of which corresponds to a fluid, with opposite signs of the level set function ϕ. It can be found that the continuous updating of ϕ is equivalent to the advection of the interface by the equation

$$\phi_t + \mathbf{v} \cdot \nabla\phi = 0 \quad (7)$$

where $\mathbf{v}$ is the advection velocity of the level sets. In practice, the level sets are only updated in the near interface region, which usually includes the first and second nearest cell-layers. For the region far from the interface the level sets are re-initialized (Susseman et al 1998) by the equation

$$\phi_\tau + \mathrm{sgn}(\phi)\left(|\nabla\phi| - 1\right) = 0, \quad (8)$$

where $\mathrm{sgn}(\phi)$ is a sign function, to maintain the signed distance property of level set function.

Interface reconstruction

The cell-face apertures are calculated by assuming a linear distribution of the level set along the cell face. By including the information on the level set normal direction a prediction of the two-dimensional volume fraction can be given as

$$H(\phi,\varepsilon) = \begin{cases} 0 & \text{if } \Lambda > \Gamma, \quad \phi < 0 \\ \frac{1}{2} + \frac{1}{\varepsilon^2}D\phi + \frac{1}{2}\frac{\Lambda^2}{\varepsilon\Gamma} & \text{if } \Gamma \geq \Lambda \geq 0, \quad \phi < 0 \\ \frac{1}{2} + \frac{1}{\varepsilon^2}D\phi & \text{if } \Lambda < 0 \\ \frac{1}{2} + \frac{1}{\varepsilon^2}D\phi - \frac{1}{2}\frac{\Lambda^2}{\varepsilon\Gamma} & \text{if } \Gamma \geq \Lambda \geq 0, \quad \phi > 0 \\ 1 & \text{if } \Lambda > \Gamma, \quad \phi > 0 \end{cases} \quad (9)$$

in which $D = \varepsilon \min(\frac{1}{|N_x|}, \frac{1}{|N_y|})$, $\Gamma = \sqrt{D^2 - \varepsilon^2}$ and $\Lambda = \frac{\Gamma}{2} + \frac{D|\phi|}{\varepsilon} - \frac{\varepsilon}{2}$. The above smoothed Heaviside functions are symmetric to $\phi = 0$ returning a volume fraction of 0.5. For a

given fluid all the cells can be classified into three types: cells with volume fraction larger than 0.5 are normal cells, cells with volume fraction less than 0.5 but non-zero are small cells, and otherwise they are empty cells.

A mixing procedure

For a small or empty cell, a stable fluid state may not be obtained based on the time step calculated according to the full grid size CFL condition. Therefore, it is suggested that the fluid in those cells should be mixed with that of their neighboring cells. As the targeted neighboring cells are preferred to be normal cells, they are determined from the level set normal direction.

The changes of the conservative quantities in the x and y directions for the small cells and the targeted cells after a mixing operation are calculated according to the averaged conservative quantities. Then the conservative quantities for one fluid in the near interface cells are updated by

$$\alpha_{i,j}^{n+1}\mathbf{U}_{i,j}^{n+1} = \left(\alpha_{i,j}^{n+1}\mathbf{U}_{i,j}^{n+1}\right)^{*} + \sum_{k}\mathbf{M}^{x} + \sum_{l}\mathbf{M}^{y} \quad (10)$$

where $\left(\alpha_{i,j}^{n+1}\mathbf{U}_{i,j}^{n+1}\right)^{*}$ are the conservative quantities at time step $n+1$ before mixing. Here, the second and third terms on the right hand side are the summations taken for all the mixing operations in the x and y directions, respectively. Note that the present mixing procedure treats vanished and newly created empty cell automatically. For the former case, the residual conservative quantities are all transported to target cells and, for the latter case all the conservative quantities in a newly created small cell are transported from its target cells.

Interface exchanges

To obtain the momentum and energy exchanges across the interface, the proposed Riemann problems associated with interface interactions are solved on the grid points within near interface region band along the interface normal direction. After the interface interaction has been solved the interface pressure p_I and the normal velocity $\mathbf{v}_I \equiv (u_I, v_I)$ are obtained. Hence, for the fluid corresponding to $\phi > 0$, the momentum and energy transferred to it are

$$\hat{\mathbf{X}}^{\mathbf{P}}(\Delta\Gamma) = p_I\Delta\Gamma\mathbf{N}_I \quad \text{and} \quad \hat{X}^{E}(\Delta\Gamma) = p_I\Delta\Gamma\mathbf{N}_I\cdot\mathbf{v}_I, \quad (11)$$

respectively. Here $\Delta\Gamma$ and $\mathbf{N}_I$ are the interface segment length or area and normal direction, respectively. $\hat{\mathbf{X}}^{\mathbf{P}} = (\hat{X}_x^{\mathbf{P}}, \hat{X}_y^{\mathbf{P}})$ stands for the transferred momentum in the respective x and y directions and $\hat{X}^E$ stands for the transferred energy. Note that there is no exchange of the tangential momentum and energy, which ensures the present method recovering exact discontinuities of tangential velocity on the interface. Also note that since the momentum and energy transferred between the two fluids have the same values but opposite sign, the overall conservation property is therefore satisfied.

LOW-DISSIPATION WENO SCHEME

In the present method, the flow field of individual fluids is solved by the single-phase characteristic WENO-LLF scheme (Jiang and Shu, 1996) and TVD Runge-Kutta scheme for time integration (Shu and Osher, 1988). The WENO($2r-1$) scheme can be described in the context of one-dimensional advection equation

$$\frac{\partial u}{\partial t} + \frac{\partial}{\partial x}f(u) = 0. \quad (12)$$

Eq. (1) is discretized in the spatial domain such that $x_i = i\Delta x$, in which Δx is the cell size, and $u_i = u(x_i)$. The semidiscretized form of Eq. (1) is

$$\frac{du}{dt} = -\frac{1}{\Delta x}\left(\hat{f}_{i+1/2} - \hat{f}_{i-1/2}\right), \quad (13)$$

in which $\hat{f}_{i+1/2}$ and $\hat{f}_{i-1/2}$ are a numerical approximation of the fluxes at the right and left cell faces. Once the right-hand side of this expression has been evaluated, TVD Runge-Kutta methods are employed to advance the solution in time. The numerical flux at the cell face is computed by a flux-splitting method

$$\hat{f}_{i+1/2} = \hat{f}_{i+1/2}^{+} + \hat{f}_{i+1/2}^{-}, \quad (14)$$

in which $\hat{f}_{i+1/2}^{+}$ and $\hat{f}_{i+1/2}^{-}$ are the positive and negative fluxes, respectively. These fluxes are interpolated with the underlying numerical fluxes, i.e. the local Lax-Friedrichs (LLF) fluxes, calculated with the nearby cell averages.

Specifically, for example, $\hat{f}_{i+1/2}^{+}$ is built through the convex combination of a number of values calculated from the candidate interpolate functions $\hat{f}_k^{+}(x)$ reconstructed from upwind rth order stencils,

$$\hat{f}_{i+1/2}^{+} = \sum_{k=0}^{r-1}\omega_k\hat{f}_k^{+}\left(x_{i+1/2}\right). \quad (15)$$

Here, the interpolated values are obtained by summations with tabulated coefficients, i.e. $\hat{f}_k^{+}\left(x_{i+1/2}\right) = \sum_{j=0}^{r-1}c_{kj}\hat{f}_{i-k+j}^{+}$, and the weights ω_k are normalized from α_k defined as

$$\alpha_k = \frac{d_k}{(\beta_k+\epsilon)^p} \quad (16)$$

in which the d_k are called the optimal weights since they generate the $(2r-1)$th order central upstream scheme, $\epsilon > 0$ prevents division by zero, β_k are the smoothness indicators defined by

$$\beta_k = \sum_{k=1}^{r-1}\Delta x^{2k-1}\int_{x_{i-1/2}}^{x_{i+1/2}}\left(\frac{d^k}{dx^l}\hat{f}_k^{+}(x)\right)^2 dx \quad (17)$$

which become large when discontinuities are present within the candidate stencil, and $p = 1$ or 2 is chosen to adjust the distinct weights at non-smooth parts of the solution.

Similarly, $\hat{f}_{i+1/2}^{-}$ can be computed by shifting the stencils one grid point to the right and reverse the upwind direction. Note that, although the optimal weights give the $(2r-1)$th order central upstream scheme for the individual positive and negative fluxes, they actually generate the standard $2r$th central scheme for $\hat{f}_{i+1/2}$ in Eq. (13) due to the flux-splitting combination of Eq. (14) (Kim and Kwon 2005).

Reference smoothness indicator

Although the weights defined in Eq. (16) show very good properties in shock-capturing, it is found that they triggers adaption too readily and thereby causes unnecessarily degradation of performance. To overcome this difficulty, Borges et al. (2008) suggest another form of weighting specifically for WENO5 ($r = 3$) scheme

$$\alpha_k = d_k\left[1 + \left(\frac{\tau_5}{\beta_{3,k}+\epsilon}\right)\right], \quad k = 0, 1, 2. \quad (18)$$

where $\beta_{3,k}$ is the classical kth smoothness indicator of 3rd order stencils and $\tau_5 = |\beta_{3,0} - \beta_{3,2}|$ which gives a higher-order smoothness indicator, and is supposed much smaller than $\beta_{3,k}$ in moderate float field. In fact, Eq. (18) can be explained by a normalization of the classical smoothness indicators with a reference value. Since τ_5 is a combination of the smoothness indicators for the 3rd order stencils, it is not clear whether or how similar combinations can be found for WENO schemes with other order of accuracy.

In order to extend the idea of reference smoothness indicator for WENO schemes with arbitrary order of accuracy, we define the following weights

$$\alpha_k = d_k \left(a + \frac{\beta_{2r-1,0}}{\beta_{r,k} + \epsilon} \right), \tag{19}$$

in which $a = 10$, β_k^r are classical smoothness indicator of the rth order stencils and the reference value $\beta_{2r-1,0}$ is the smoothness indicator of the optimal $(2r-1)$th order stencil. Note that the increase of computational complexity and cost for calculating $\beta_{2r-1,0}$ is minor. The basic idea is that, since the weights intend to adapt themselves between those of the candidate stencils and the optimal stencil, a straightforward choice of the reference smoothness indicator is that of the optimal stencil. With this choice, in moderate float field the value $\beta_{2r-1,0}$ with vanishing high-order derivatives is close to $\beta_{r,k}$, hence produces less distinction of weights form the optimal values. To ensure the dominant of the optimal stencil when its smoothness indicator is comparable with those of the candidate stencils, a large value of a is used in Eq. (19).

VALIDATING TESTS

In the following two one-dimensional examples are provided to illustrate the potential of the proposed method. We use the modified 5th-order WENO-LLF scheme and a 3rd-order TVD Runge-Kutta scheme for spatia and integration, respectively. All the computations, if not mentioned otherwise, are carried out with a CFL number of 0.6.

Wave-interface interaction

We consider a wave-interface interaction problem with the following initial conditions

$$(\rho, u, p, \gamma) = \begin{cases} (1, 0.5\sin[\pi(1-0.5x)], 1, 1.4) & \text{if } x < 0.5 \\ (1, 0.5\sin[\pi(1-0.5x)], 1, 1.8) & \text{if } x > 0.5 \end{cases}$$

and reflecting wall boundary condition applied at both $x = 0$ and $x = 1$. The case is computed up to time $t = 1$. We examine the numerical solutions with the reference "exact" solution computed with 1600 grid points. Figure 2 shows the calculated velocity and density profiles at time $t = 0.25$ and 0.75. One can observe that the computed results are in good agreement with the "exact" solution.

Resolution studies are carried out to measure the numerical convergence rate of the method. We measure the entropy errors $E_s = |s^t - s^{exact}|/s^{exact}$ at $t = 0.2$ and 0.64 corresponding to the time when the entropy assumes the extreme value in a continuous flow or when the shock waves pass the interface. The entropy errors E_{s-} and E_{sT} for the left and total medium, respectively, and the averaged order of convergence R_c are given in Table 1. One can find that high-order accurate results are obtained for the continuous flow. However, when there is a shock wave and especially when the shock wave passes the interface, larger errors are

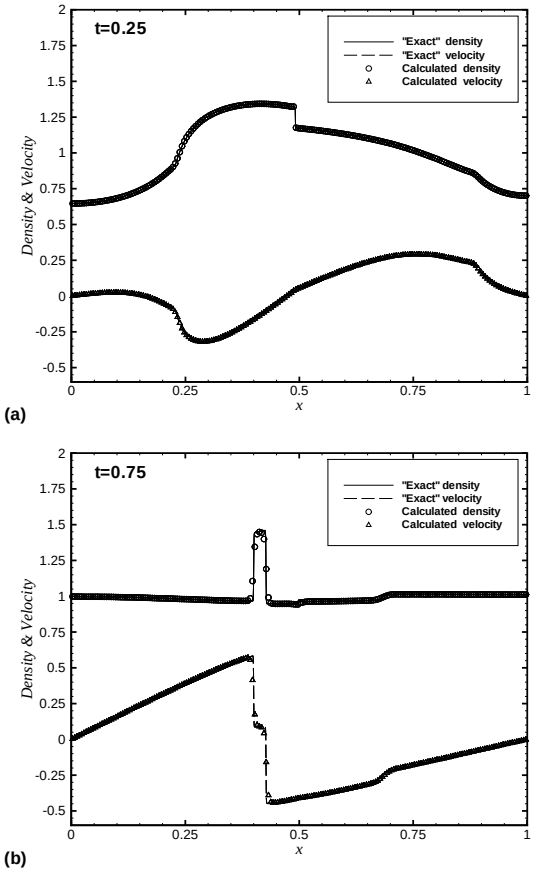

Figure 2: Wave-interface interaction.

Table 1: Errors and convergence rate the case of wave-interface interaction .

$1/h$	$E_{s-}^{t=0.2}$	$E_{sT}^{t=0.2}$	$E_{s-}^{t=0.64}$	$E_{sT}^{t=0.64}$
50	3.7×10^{-4}	4.1×10^{-4}	5.2×10^{-3}	4.9×10^{-3}
100	2.6×10^{-5}	9.2×10^{-5}	2.1×10^{-3}	2.1×10^{-3}
200	4.9×10^{-6}	2.4×10^{-5}	7.1×10^{-4}	9.0×10^{-4}
400	4.0×10^{-7}	5.7×10^{-6}	1.2×10^{-4}	3.5×10^{-4}
R_c	3.3	2.5	1.8	1.3

produced with an order of convergence decreasing towards unity.

Shock-density-wave interaction

For the shock entropy wave interaction problem (Shu and Osher 1988) the initial conditions are set by a Mach 3 shock interacting with a perturbed density field:

$$(\rho, u, p, \gamma) = \begin{cases} (3.857, 2.629, 10.333, 1.4) & \text{if } 0 \le x < 1 \\ (1 + 0.2\sin(5x), 0, 1, 1.4) & \text{if } 10 \ge x > 1 \end{cases}$$

with zero-gradient boundary condition at $x = 0$ and 10. The solution of this problem consists of a number of shocklets and fine scales structures which are located behind a right-going main shock. Fig. 3a and b gives the calculated density and velocity profile at $t = 1.8$ with an increasing number of points. We shall refer to the solution computed by the modified WENO scheme with 1600 points as the "exact" solution. At a low resolution, N = 200, as shown in Fig. 3a, the modified WENO capture much more fine scale

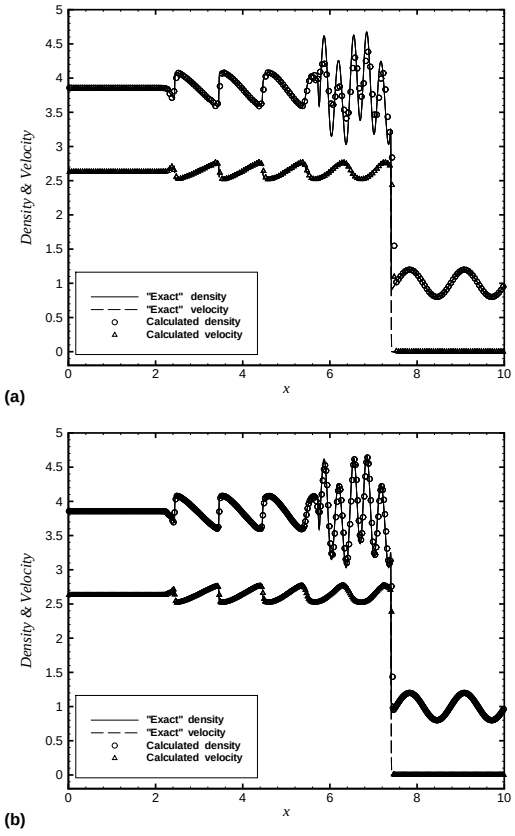

Figure 3: Shock-density-wave interaction: (a) N=200, (b) N = 400.

structures of the solution than the original scheme, particularly at the high-frequency waves behind the shock. Note that the present method is able to achieve comparable small dissipation as hybrid methods, like Kim and Kwon (2005).

SIMULATION RESULTS

We study the two-dimensional nonlinear evolution of inviscid KH instability with different convective Mach number. The initial data are

$$(\rho, u, p, \gamma) = \begin{cases} (\rho_u, \frac{1}{2} + \widetilde{u}, \widetilde{v}, p_0, \gamma_u) & \text{upper fluid} \\ (\rho_b, -\frac{1}{2} - \widetilde{u}, \widetilde{v}, p_0, \gamma_b) & \text{lower fluid} \\ \phi = -0.5 + y & \text{level set} \end{cases}$$

in a $[0,1] \times [0,1]$ domain. The initial perturbation is introduced by modifying slightly the velocity profile in a thin layer beside the tangential velocity discontinuity, i.e. the velocity fluctuations are

$$\widetilde{u} = \frac{1}{10}\cos(2k\pi(x - \frac{1}{2}))\exp(-2k\pi|y - \frac{1}{2}|)$$
$$\widetilde{v} = \frac{1}{10}\sin(2k\pi(x - \frac{1}{2}))\exp(-2k\pi|y - \frac{1}{2}|).$$

Different convective Mach number $M_c = \sqrt{\frac{\gamma_u p_0}{\rho_u}}$ is achieved by adjust the initial pressure value p_0. Different density ratio $\rho_c = \frac{\rho_u}{\rho_b}$ and specific-heat-ratio ratio $\gamma_c = \frac{\rho_u}{\rho_b}$ are achieved by adjust the density and specific heat ratio of the lower fluid. The computation is carried on a 200×200 mesh. Horizontal periodic boundaries and vertical slip-wall boundaries are used.

Fig. 4 gives the computed interface position and vorticity profile at $t = 4$ for the case with convective Mach number

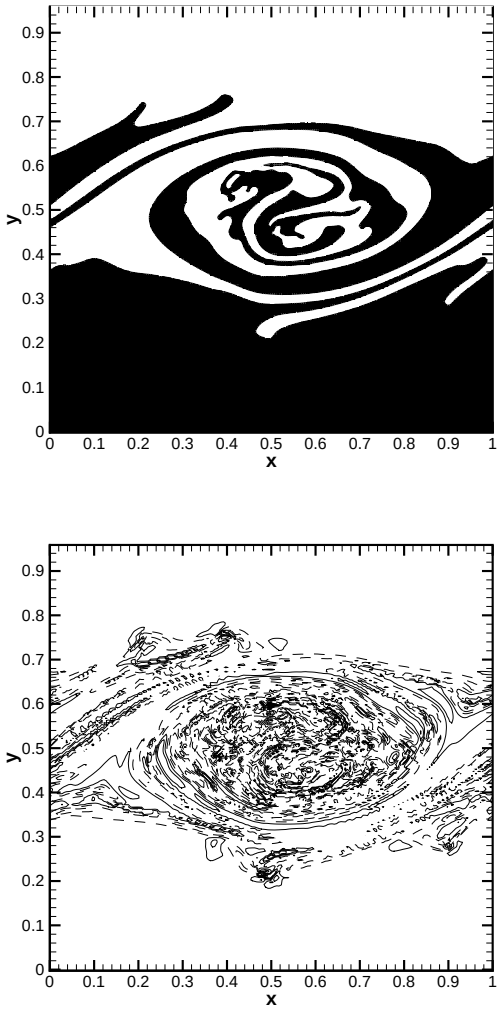

Figure 4: Case $M_c = 0.387$, $\rho_c = 1, \gamma_c = 1$ at $t = 4$: interface (left) and vorticity (right).

$M_c = 0.387$, density ratio $\rho_c = 1$, γ ratio $\gamma_c = 1$ and single mode perturbation. Comparing to the results of a previous work of Després and Lagoutière (2007) with the single fluid model, the general features are in good agreement. However, the current results show much more detailed structure than their results with a 500×500 grid. This is not unexpected because their method suppressed the development of the high-wave-number disturbances, which can only partly shown in their results on a 1000×1000 grid. Another notable observation is that, even the prescribed perturbation is single mode with the wave length of the domain, the high-wave-number disturbances due to slightly initial numerical errors on velocity profile are not suppressed and develop quickly in the early stage, as shown by the heavily winkled interface in Fig. 5. However, these disturbances seem not grow up further and are smoothed in the later stage, as shown in Fig. 4. This is quite different from the previous simulations with vortex point method (Krasny 1986), in which the high-wave-number disturbances grow up uncontrollably if the artificial viscosity is not sufficiently high. One can find that the vorticity field is quite noisy, which suggests that a large portion of small scale vortices have been

diffused off the interface. Since there is no direct mechanism for vorticity diffusion in our numerical method, it can be explained as the baroclinic production due to the mismatch between the pressure and the density gradients near the interface, when the highly winkled interface can not be resolved by the level sets. As the vorticity being diffused off the interface, a shear layer with increasing thickness is produced which intend to suppress the the growth rate of high-wave-number disturbances. On the other hand, the interface is flattened by stretch of the interface, i.e. the rolling-up due to the development of prescribed single mode perturbation. These phenomena suggest that, though the high-wave-number disturbances initially develop fast, their growth rate decrease fast too because of dissipation mechanism, and the high-wave-number instabilities are smeared by the low-wave-number instabilities.

The influence of the compressibility on the growth rate is shown in Fig. 5. One can find, if the upper and lower

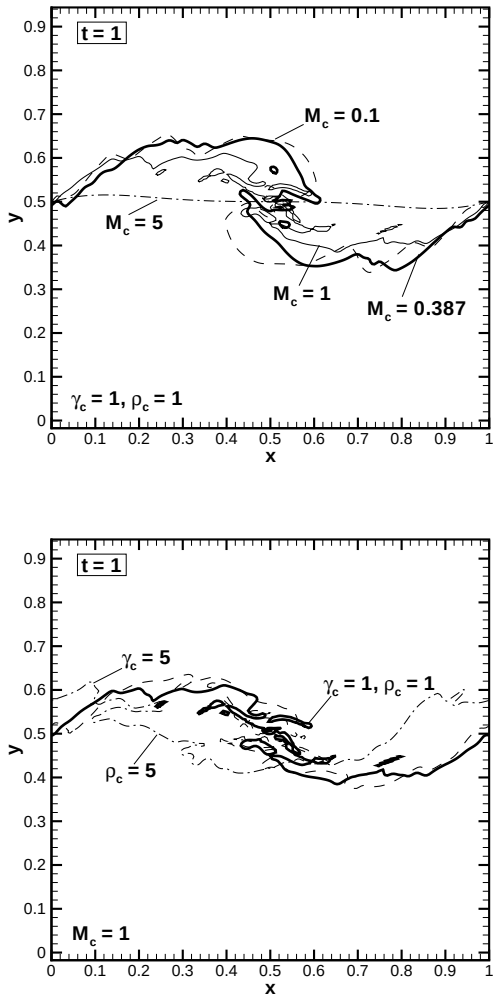

Figure 5: Interface at different M_c (left) and different γ_c or ρ_c (right).

fluids have the same compressibilities (with the same densities and specific heat ratios), the growth rate of the single mode perturbation decreases monotonically with M_c to almost zero when $M_c = 5$. This behavior is consistent with the linear theory on shear layer with finite thickness, but inconsistent to that of the idea KH instability. However, for the disturbances with higher wave number, if $M_c < 1$, the growth rate increases with M_c, and then decreases to almost zero when $M_c = 5$. This behavior is consistent with the linear theory of the idea KH instability. If the upper and lower fluids have different compressibilities (by increasing the density or specific heat ratio of the lower fluid), one can find that, while the growth rate of the single mode perturbation does not change much, that of the disturbances with higher wave number generally decreases, which again suggests that higher-wave-number disturbances can grow faster with the increase of M_c.

CONCLUDING REMARKS

In this paper, a sharp-interface method combined with a low-dissipation WENO scheme is introduced to simulate the compressible KH instability. The simulations show that, though this method allows the development of high-wave-number perturbation, the high-wave-number perturbation shown different behavior from previous simulations and linear theory on idea KH instability but resemble those on shear layer with finite thickness.

REFERENCES

Borges, R., Carmona, M., Costa, B., and Don, W.S., 2008 "An improved weighted essentially non-oscillatory scheme for hyperbolic conservation laws", *J. Comput. Physics*, Vol. 227, pp. 3191-3211.

Després, B., and Lagoutière, F., 2007 "Numerical resolution of a two-component compressible fluid model with interfaces", *Progress in Computational Fluid Dynamics*, Vol. 7, pp. 295-310.

Hu, X. Y., Khoo, B. C., Adams, N., and Huang, F. L. 2006 "A conservative interface method for compressible flows", *Journal of Computational Physics*, Vol. 219, pp. 553-578.

Jiang, G. S., and Shu, C. W., 1996 "Efficient Implementation of Weighted ENO Schemes', *Journal of Computational Physics*, Vol. 126, pp. 202-228.

Kim. D., and Kwon, J. H, 2005 "A high-order accurate hybrid scheme using a central flux scheme and a WENO scheme for compressible flowfield analysis", *Journal of Computational Physics*, Vol. 210, pp. 554-583.

Krasny. R., 1986 "Desingularization of periodic vortex sheet roll-up", *Journal of Computational Physics*, Vol. 65, pp. 292-313.

Miller, G. H., and Colella, P., 2001 "A conservative three-dimensional Eulerian method for coupled solid-fluid shock capturing", *Journal of Computational Physics*, Vol. 183, pp. 26-82.

Osher, S., and Sethain, J. A., 1988 "Front propagating with curvature dependent speed: algorithm based on Hamilton-Jaccobi formulation", *Journal of Computational Physics*, Vol. 79, pp. 12-49.

Schmitt, C., Hu, X. Y., and Adams, N. A., 2007 "Vorticity Production and Mixing in Shock Bubble Interaction", *International Workshop "Turbulent Mixing and Beyond," TMBW-07*, Trieste, Italy, August 18-26, 2007.

Shu, C. W., and Osher, S., 1988 "Efficient implementation of essentially non-oscillatory shock-capturing schemes", *Journal of Computational Physics*, Vol. 77, pp. 439-471.

Sussman, M., Fatemi, E., Smereka, P., and Osher, S. 1998 "An improved level set method for incompressible two-phase flows", *Computers and Fluids* Vol. 27, pp. 663-680.